ADVANCED MATERIALS
www.advmat.de

Polymer/Perovskite Amplifying Waveguides for Active Hybrid Silicon Photonics

Isaac Suárez, Emilio J. Juárez-Pérez, Juan Bisquert, Iván Mora-Seró, and Juan P. Martínez-Pastor**

Hybrid halide perovskites (HPVKs)[1] have emerged as an outstanding material for photovoltaic applications[2,3] with certified efficiencies higher than 20%.[4] Although solar cells are the dominant research trend, HPVKs have been successfully employed in photodetectors[5] and show excellent light emitting properties, as investigated in the 1990s,[6,7] and more recently for light-emitting diodes (LEDs),[8,9] white light emitters,[10] and lasing devices.[11–14] The development of HPVK photonic applications will require efficient and stable devices capable of being incorporated in silicon circuitry. The new amplifiers and receivers architectures based on HPVKs could be optimal for the growing field of short-distance data communications using plastic optical fibers.[15] Here, we report the use of HPVKs as gain materials in a planar waveguide configuration integrated on a silicon substrate and cladded by a poly(methyl methacrylate) (PMMA) polymer, also acting as a passive cladding of the bilayer waveguide. We have designed a solution processed optical amplifier, as demonstrated by the production of amplification of the spontaneous emission (ASE) at 780 nm above an energy threshold as low as 2 nJ pulse^{-1}, with a net gain of around 10 dB cm^{-1} under nanosecond pulsed laser excitation; simultaneously the linewidth of the waveguided light reduces from 50 (spontaneous emission regime) down to 3–4 nm (ASE regime). Samples were prepared by a low cost solution processing method and no degradation of the device has been observed after more than one year. These results pave the road toward very efficient active HPVK photonics in silicon and other substrates.

Despite the polycrystalline nature of HPVK thin films, the punctual defects with the lowest formation energy, which produce shallow traps and even grain boundaries, do not lead to the formation of middle gap deep traps.[16] These properties are fundamental to reducing nonradiative recombination channels and hence to envisaging direct gap HPVKs as promising semiconductors for photonic applications. Firstly, they are highlighted as very efficient light emitters, as derived from their direct bandgap semiconductor nature and negligible influence on nonradiative centers that leads to a high photoluminescence (PL) quantum yield of ≈70% at room temperature.[11] Second, a broad variety of HPVK materials can be synthesized with different bandgap values in the visible to near infrared region, by just changing the components of the ABX_3 perovskite structure.[7,9,17] Here, we have used as an active layer $CH_3NH_3PbI_3$ perovskite. Despite the attractiveness of the material, only a relatively small number of works have been developed very recently in the field of photonic and emitting optoelectronic devices. The generation of optical gain is of particular interest since it is the basis of the practical implementation of solid-state lasers and amplifiers integrated on silicon-based platforms.

Different materials have been proposed as a gain medium in the last years, especially that can be solution-processed, which are particularly convenient for low cost devices in order to be integrated with Si and other substrates. For example, organic semiconductors[18,19] or colloidal quantum dots (QDs)[20,21] have been employed to demonstrate integrated amplifiers and lasers, but they present some drawbacks. Organic materials show limited wavelength tunability, bad heat conductivity and bleaching, while most of the QD-based nanomaterials suffer from important nonradiative Auger losses (≈10 ps) implying the necessity of femtosecond pulsed laser excitation to achieve population inversion. In this context, HPVKs emerge as a brilliant future candidate for Si-hybrid photonics to overcome most of the above negative issues since they exhibit fast carrier formation (≈1 ps),[12] high quantum yield,[11,12] and relatively long recombination times at room temperature (≈10 ns).[19] In fact, these primary properties were exploited to demonstrate ASE in a simple dropped-casting layer on a quartz substrate[12] or a cholesteric liquid crystal cavity[22] and lasing action in a nanowire shape,[23] and when the HPVK was embedded in a vertical photonic cavity structure[11] or deposited on silica microspheres.[14] In these publications the optical pumping was carried out by short pulsed lasers; femtosecond[11] to demonstrate ASE or lasing in nanowires,[23] and picosecond/nanosecond when the HPVK was incorporated into a resonator.[11,12] These pumping conditions are necessary to reduce Auger recombination (≈100 ps) and provide enough peak power to overcome the stimulated emission threshold (10–65 μJ cm^{-2}).[11–14] These previous works established an important milestone demonstrating ASE behavior. However, it is still necessary to develop an optimized low cost technology to integrate efficiently HPVK into photonic devices by assuring also device stability, and minimizing the pump energy threshold in order to reduce their power consumption.

Dr. I. Suárez, Prof. J. P. Martínez-Pastor
UMDO, Instituto de Ciencia de los Materiales
Universidad de Valencia
46071 Valencia, Spain
E-mail: Juan.Mtnez.Pastor@uv.es
Dr. E. J. Juárez-Pérez, Prof. I. Mora-Seró
Institute of Advanced Materials (INAM)
Universitat Jaume I
12006 Castelló, Spain
E-mail: sero@uji.es
Prof. J. Bisquert
Department of Chemistry
Faculty of Science
King Abdulaziz University
Jeddah 21589, Kingdom of Saudi Arabia

DOI: 10.1002/adma.201503245

ADVANCED MATERIALS
www.advmat.de

www.MaterialsViews.com

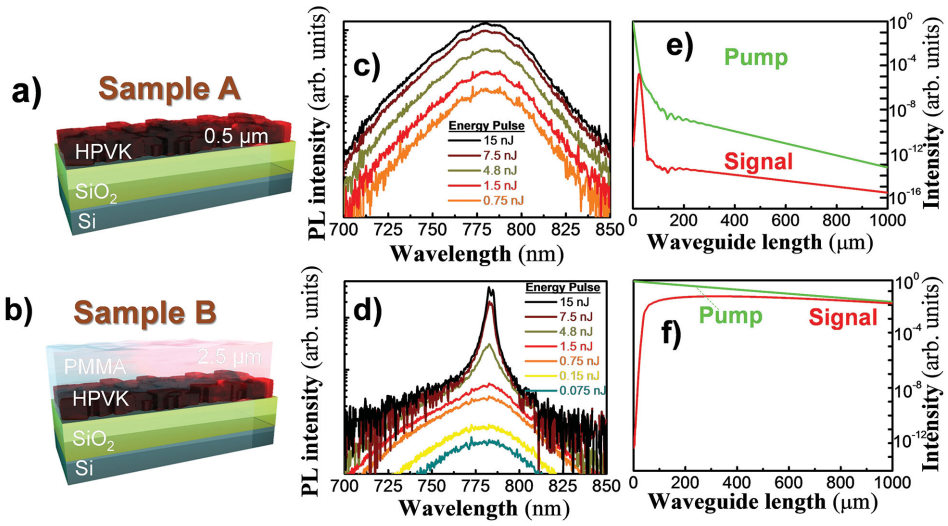

Figure 1. a) Sample A structure: A thin layer of HPVK (500 nm) is deposited by spin coating on a Si/SiO_2 substrate, a previous buffer of TiO_2 was deposited on SiO_2 to enhance HPVK adherence. b) Sample B structure: similar to sample A, but adding a PMMA cladding layer (2.5 μm) on top of the HPVK. c,d) PL spectra for different pump powers in samples A and B, respectively. e) Simulation of pump (green line) and signal (red line) light propagation along the waveguide in sample A: the pump is strongly attenuated at the input edge of the waveguide and hence, appreciable signal is only generated along the first 50 μm. f) Simulation of pump (green line) and signal (red line) intensities along the waveguide in sample B: the pump travels along the entire waveguide with the aid of the cladding, improving the PL (signal) excitation along the entire sample.

Here we propose a smart solution for the aforementioned requirements by the development of optical waveguides using a thin HPVK layer, see **Figure 1**a, and HPVK layer cladded with PMMA polymer, see Figure 1b, both deposited by spin-coating onto a Si/SiO_2 substrate (the most widely used for photonics). If the thickness of the PMMA is appropriate, the light emitted by the HPVK will be coupled to waveguided optical modes leading to the generation of ASE. This regime is reached at a relatively low threshold due to the confinement of pump and signal light beams in the optical waveguided mode. Interestingly, the PMMA cladding layer plays a double role: it allows the efficient confinement and propagation of pump and signal beams, and importantly, provides the encapsulation of the gain material, HPVK, ensuring long-term stability. With this configuration, Figure 1b, we have demonstrated the production of ASE at 780 nm (the PL peak wavelength) with a linewidth of around 3 nm (as compared to the 50 nm wide PL band) for laser pumping above an energy threshold as low as 2 nJ (30 μW of average power) inside the waveguide. This value is an estimate by assuming a 10% of coupling efficiency of the pumping laser focused at the entry face of the waveguide (i.e., 300 μW), in agreement with the theoretically estimated value, as discussed below. This low power threshold is especially significant taking into account that excitation is produced with a nanosecond pulsed laser instead of picosecond or femtosecond ones. We have carefully analyzed by experiments and simulations the generation of optical gain in the waveguide structure. We have estimated a net gain, at the output edge of the waveguide, of the order of 10 dB cm^{-1} for 1 mm long waveguides. These results pave the road toward very efficient active HPVKs photonics, amplifiers and lasers, into Si-based integrated architectures.

Two different slab waveguide configurations have been adopted, with and without the PMMA cladding layer, Figure 1a,b, respectively, named hereafter sample A and sample B. Briefly, on a Si/SiO_2 substrate (2 μm of SiO_2), an intermediate 40 nm thick TiO_2 buffer layer is deposited to enhance the HPKV adhesion. HPVK films of different thicknesses (Figure S1, Supporting Information) were deposited by spin coating on top of the TiO_2 buffer layer, see the Experimental Section for more details. For this configuration, in sample A (Figure 1a), the HPVK film would act as the active core of the planar waveguide, given that the refractive index of the HPVK is around 2.34 at 780 nm, much higher than the one of SiO_2 (see Table S1, Supporting Information). However, the propagation of a pumping laser beam along this single layer waveguide is restricted to short distances due to the strong absorption of the HPVK material above its bandgap, see Figure S3b, Supporting Information. In fact, when the optical pumping laser (λ_p = 533 nm) is coupled to the HPVK waveguide the excitation is limited to very short distances of ≈100 nm due to the strong attenuation of the pump beam (the absorption of guided modes are about 10^5 cm^{-1}, see Figure S5b, Supporting Information). In consequence, for a practical waveguide length of ≈1 mm the generation of emitted light for sample A cannot overcome the intrinsic losses of the structure and no ASE is obtained in the range of pumping energies 0.75–15 nJ (inside the waveguide), as shown in Figure 1c. On the contrary, the use of a PMMA cladding layer on top of the HPVK in sample B (Figure 1b) enables end-fire coupling of the excitation laser through the planar PMMA–HPVK waveguide with calculated weak losses in the range 10–100 cm^{-1} (see Figures S4b and S5b, Supporting Information). As a consequence, a clear signature of ASE for sample B configuration is plainly visible by increasing the laser pumping energy above 2 nJ, i.e., the waveguided PL signal collapses into a narrow emission line at 1.58 eV (780 nm), as observed in Figure 1d.

Adv. Mater. **2015**,
DOI: 10.1002/adma.201503245

Furthermore, it is important to highlight that the PMMA acts also as encapsulation of the HPVK layer against ambient conditions, preserving the device performance for many months (to date more than one year of optical tests in laboratory) stored under ambient conditions (see Figure S7, Supporting Information, for a comparison of the spectra obtained immediately after the fabrication and 10 months later). In the case of only HPVK planar waveguides (sample A) the emitted light was completely quenched only one week after fabrication and exposed to ambient conditions.

For a deeper understanding of the ASE production in the proposed waveguides a generation-recombination model has been developed (see Section 4, Supporting Information, for a more detailed description). Nonradiative channels in $CH_3NH_3PbI_3$ have been deeply studied by Manser and Kamat,[24] concluding that electron–hole recombination is dominant and Auger recombination is considered negligible, for excitation levels similar than those used in our experiments. Other nonradiative channels studied in previous publications[19] are bulk and interfacial/surface traps whose density is in the order of $\approx 10^{16}$–10^{17} cm^{-3} and hence these channels have no influence under high pumping excitations.[25] We have taken into account all these considerations in the model, which allows us to simulate the pump and signal intensities along the waveguide for both samples A and B, see Figure 1e,f, respectively. These figures show the evolution of the pump beam at $\lambda = 533$ nm (green line) and signal at $\lambda = 780$ nm (red line) simulated by a beam propagation method (BPM).[26] The simulation predicts that sample A suffers from a strong attenuation characterized by three exponential decay regions: the first one attributed to the absorption losses of the HPVK (1.3×10^5 cm^{-1}) and the other two to radiated losses to the substrate (130 cm^{-1}) and to the air (1000 cm^{-1}). On the contrary, the pump beam in sample B exhibits a very weak attenuation accounted for by a single decay constant of 34 cm^{-1}, a value close to the losses obtained for the modes confined in the PMMA cladding in the simulations (see Figure S5b, Supporting Information). Consequently, at the waveguide exit edge, $z = 1000$ µm, the PMMA cladding produces a 10^{11}-fold enhancement of the pump intensity as compared to sample A.

The waveguided PL signal can be now estimated on the basis of the pumping beam calculated above by considering the spontaneous emission generation together with an active BPM algorithm, similar to the one applied by Gordillo et al.[27] The model allows obtaining the optical gain by calculating the carriers generated along the structure.[28] The simulation of the signal intensity in samples A and B (red lines in Figure 1e,f) gives in both cases an initial rise due to the immediate achievement of maximum net gain at around $z = 100$–200 µm. In sample A this gain is lost after a short propagation distance because the photogeneration by light absorption decreases very fast (Figure 1e), while in sample B the losses are practically compensated along the entire waveguide, as the pump signal is only weakly attenuated in this case (Figure 1f).

The highest gain is obtained with a PMMA thickness of around 2.5 µm, see Table S2 in the Supporting Information, as a good compromise between propagation losses and excitation of the HPVK material along the propagation length (see Figures S4 and S5, Supporting Information). Using this PMMA thickness, the structure supports a propagating optical mode centered in the PMMA (see Figure S6, Supporting Information) for the pumping laser wavelength; this mode is characterized by a propagation length of around 400 µm and an overlapping percentage with the active region close to 0.02% (Figure S5, Supporting Information). Despite this low overlap value, it is worth noting that PL is generated along the entire length of the waveguide and the cladding PMMA is recovering radiated light that enhances considerably the amount of guided PL signal. **Figure 2**a shows the intensity distribution of the pump and signal beams simulated with BPM in a sample with the optimum geometrical parameters. Clearly, the pump beam travels along the polymer cladding while the signal beam is confined in the HPVK layer, which is experimentally corroborated in Figure 2b. In addition, the pump beam shows an overlap with the active region of 0.02–0.04%, very close to the simulation (Figure 2c).

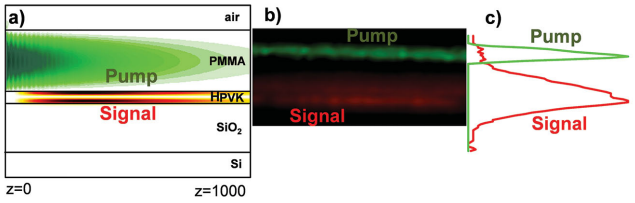

Figure 2. a) Simulation of the intensity distribution of the pump (green) and signal (red-yellow) beams along the waveguide (see also Section 4, Supporting Information, regarding the generation-recombination model). b) CCD image recorded at the output edge of a waveguide with a 3 µm thick PMMA layer showing pump (green) and signal (red) beams. c) Cross-section intensity profiles from the CCD image, where the distance between signal and pump profile peaks should be 1.75 µm (the wider cross section of the signal is attributed to radiated light caught by the PMMA cladding).

The propagation of the pump beam in sample B produces the generation of carriers along the entire length of the waveguide as estimated by the BPM (Figure S8a, Supporting Information). Consequently, gain will be produced in the waveguide when the excitation overcomes the threshold and ASE is observed experimentally for type B samples (**Figure 3**a,b). For pump energies below 2 nJ (threshold) the PL intensity is very broad (50 meV) and weak, whereas above the ASE threshold the intensity of the waveguided light signal grows considerably and its spectrum collapses into a narrow line (6–7 meV), as observed in Figure 1d. In Figure 3b, the signal intensity at the exit face of the waveguide as a function of the pumping energy is represented by solid circles (left axis scale). It can be nicely fitted using the already commented generation/recombination model (continuous line). A clear threshold is observed at around 2 nJ above which the intensity follows a linear dependence (a slope two in a log–log plot) due to ASE. The pump power inside the waveguide was considered to be around 10% of the energy of the incident laser energy (0–150 nJ), because of the difference between the spot diameter at the input edge of the waveguide (≈25 µm) and the thickness of the PMMA cladding (2.5 µm). In this way, the threshold energy density of around 100 µJ cm^{-2}, very close to the predicted value by our generation/recombination model (solid line in Figure 3b), 64 µJ cm^{-2}. Due to the high confinement of the light inside the waveguide this threshold,

ADVANCED MATERIALS
www.advmat.de

www.MaterialsViews.com

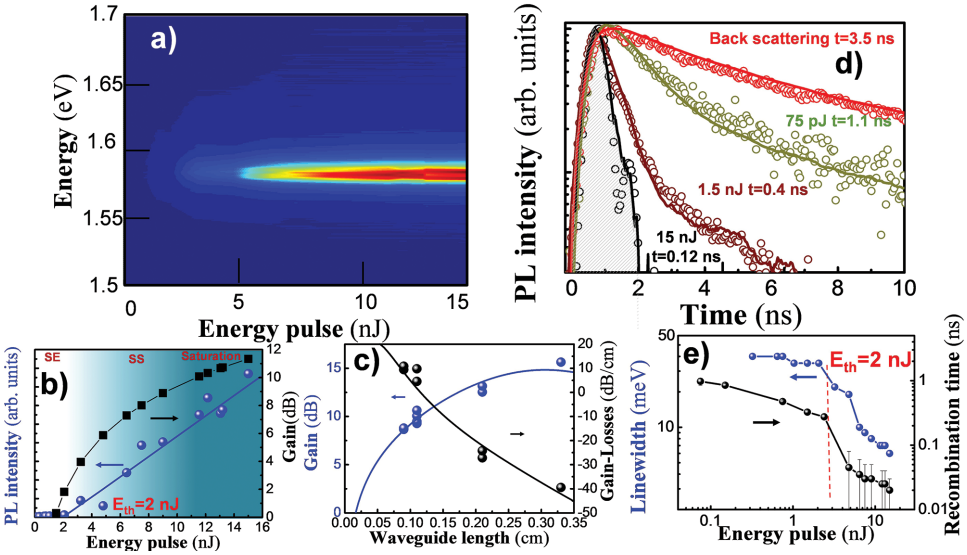

Figure 3. a) Emitted light map as a function of the pump laser energy measured at the output edge of sample B. b) Left axis (blue). Integrated waveguided PL intensity as a function of the laser pulse energy (symbols corresponds to experimental points and solid line to the fitting of BPM model). Right axis (black). Integrated gain as a function of the laser pulse energy, c) left axis (blue). Integrated gain as a function of the waveguide length (blue symbols and fitting to above-mentioned equation), right axis (black). Net gain at the output of the waveguide as a function of the waveguide length (black symbols and fitting to g-α where g follows equation given in the text). d) TRPL analysis in backscattering (red) and waveguided light configurations for different laser pulse energies; the gray dashed area corresponds to the system response. e) Linewidth (blue and left axis) and recombination time (black and right axis) as a function of the laser pulse energy; a threshold of 2 nJ is estimated (line are just an eye guides).

necessary to reach the transparency carrier concentration $n_0 = 3 \times 10^{18}$ cm^{-3} (see Section 4, Supporting Information) corresponds to an average power of 30 μW inside the waveguide (300 μW of the external pumping laser). Moreover, since the mode (confined in the PMMA) overlap in the HPVK layer is only ≈0.02%, the real pump density threshold in the active layer is hence as low as ≈20 nJ cm^{-2}, a value much smaller than the one obtained in experiments under free space optical pumping using backscattering configuration.[12,14]

Figure 3b plots the obtained experimental gain as function of energy pulse for a weveguide of 1.1 mm length. The experimental gain of the amplifier has been deduced from experimental curves by comparing the spontaneous and stimulated emission variations with power (see Section 5.2, Supporting Information). Gain increases with pump energy and saturates to around 10 dB for the highest pumping energy used in the experiments. Moreover, the experimental gain increases for longer waveguides, as observed in Figure 3c (blue solid circles, left axis). To obtain net gain, however, it becomes necessary to take into account the losses in the structure. For this purpose, 19–21 cm^{-1} losses in the waveguide have been deduced by studying the propagation of the spontaneous emission (see Section 5.3, Supporting Information). Right axis of Figure 3c plots the net gain in dB/cm for the different waveguide lengths studied here. The amplifier reaches net gains of 10 dB cm^{-1} for short length waveguides (≈1 mm).

Saturation power, P_s, and gain without saturation, g_0, result in the range of 7000–1200 photons s^{-1} and 3000–13 000 cm^{-1}, respectively, as deduced from the fitting curve to the well-know equation $g = g_0/(1+P/P_s)$ in Figure 3c (see Section 5.2, Supporting Information, for more details). The generation/recombination model predicts a maximum $g_0 \approx 4000$ cm^{-1} at the input edge of the structure, so the experimental fitting agrees reasonably well with the BPM output. This value is one order of magnitude higher than the one obtained for HPVK under free space optical pumping (100–250 cm^{-1})[12,14] and colloidal QDs (100 cm^{-1}),[20] as extrapolated from the variable length stripe method.[29] Although here the estimation is obtained by a completely different method, the high g_0 is an indication of the efficiency and effectiveness of the optical pumping method here reported. In fact, in those references the linewidth of ASE spectra was around 10 nm while in the present study it is reduced down to 3–4 nm. Furthermore, the waveguided PL spectra above threshold are completely dominated by ASE with a negligible contribution of spontaneous emission (Figure 3a), which is not the case in the aforementioned references.

As a last consideration, recombination dynamics should also be affected by the appearance of ASE in the PMMA–HPVK waveguide as observed in time resolved PL (TRPL) spectra in Figure 3d. A PL decay time of 3.5 ns is measured for the PMMA–HPVK structure under backscattering excitation–detection conditions, whereas it reduces to 1.1 ns for the waveguided PL signal under the lowest pumping conditions (75 pJ) and below 100 ps above 5 nJ. This is because gain decreases the effective decay time even below the threshold energy due to recombination-generation processes along propagation (see Section 4, Supporting Information), provided that nonradiative channels are negligible. Simultaneously, a second slow exponential decay of around ≈4–8 ns is needed to fit the experimental TRPL curves at long delay times below threshold energy that is attributed here to the remaining spontaneous emission that mostly disappears above the ASE threshold. In fact, the decay times measured at other wavelengths inside the emission band are longer than those at 780 nm, because PL is more

Adv. Mater. 2015,
DOI: 10.1002/adma.201503245

influenced by the spontaneous emission (see Figure S13, Supporting Information). In Figure 3e the linewidth and recombination time at the ASE peak (780 nm), as a function of the pump energy pulse are depicted. The onset for the decrease of the recombination time and PL linewidth narrowing clearly takes place at the energy of ≈2 nJ, in perfect agreement with the threshold value extracted from the integrated PL (Figure 3b). It is worth noting that no dependence on light polarization was observed in the production of ASE for the different studied samples obtaining the same threshold energy and line narrowing for both the pump beam and the waveguided signal (see Figure S14, Supporting Information). This is quite interesting for the application of the proposed Hybrid Semiconductor Optical Amplifier (HSOA) concept to optical communications using optical fibers where the polarization of propagating optical signals is random in nature. Finally, the influence of geometrical parameters in the structure (thickness of HPVK and PMMA films) on ASE were also investigated and summarized in Table S.1, Supporting Information, 500 nm and 2.5 μm being optimum for the HPVK and PMMA films thicknesses, respectively.

In summary, for the first time a hybrid optically active material has been integrated in cladding waveguides opening the use of hybrid lead halide perovskites for photonic applications in a silicon platform. Particularly, a high optical net gain, 10 dB cm^{-1}, has been obtained by synergistically combining the HPVK semiconductor with organic polymer waveguides. We have demonstrated a low stimulated emission threshold of 2 nJ on an optimally designed PMMA/HPVK waveguide, a decreased threshold compared to previous results,[11,12] which was remarkably obtained without requiring short pulsed lasers, i.e., a nanosecond laser, a clear indicator of the powerful waveguide approach proposed in the present work. Gain without saturation as high as g_0 = 3000–13 000 cm^{-1} at the waveguides are estimated experimentally (4000 cm^{-1} from BPM output). The excellent optoelectronic properties of HPVK are enhanced in our HSOA concept by a polymer layer that simultaneously develops two fundamental tasks: PMMA allows to propagate the pump and signal beams along suitable long distances, avoiding the strong attenuation observed in devices without it, and, also very important, to protect the HPVK layer from moisture/air degradation producing long stability devices, presenting no degradation after more than one year. Both HPVK and PMMA layers are deposited by using very simple solution processing techniques. The threshold for ASE is supported by the power dependence of the waveguided PL and TRPL spectra, and corroborated by theoretical simulation. The application of model to our experimental results also demonstrates that Auger recombination and surface traps are negligible in this kind of materials. Waveguides and other photonic devices based on HPVK/PMMA bilayer may be easily integrated into Si circuitry, assuring device stability and low power consumption due to the low energy threshold for operation.

Experimental Section

Waveguide Fabrication: Si/SiO_2 wafers were thoroughly and sequentially cleaned with acetone, ethanol and isopropanol solvents. Then the wafers were dried using a N_2 stream and heated for 1 min at 100 °C over a hot plate. A ≈40 nm thickness layer of TiO_2 was deposited on the SiO_2/Si wafer by spin-coating an anhydrous ethanol solution of titanium isopropoxide and heated at 500 °C for 30 min in room atmospheric conditions. Halide perovskite $CH_3NH_3PbI_{3-x}Cl_x$ layer of ≈500 nm of thickness was deposited inside a glove-box by spin-coating 100 μL of perovskite precursor solution, 40% (w/w) DMF solution of CH_3NH_3I and $PbCl_2$ (3:1 molar ratio),[3] onto the SiO_2/Si wafer at 2000 rpm for 60 s. After the deposition, the substrate was kept at room temperature for 15 min and then heated up to 100 °C during 1 h inside an oven under air atmosphere. Control of HPVK thickness with the 40% (w/w) solution was obtained by varying the spin-coater speed for the layer deposition, see Figure S2, Supporting Information. For the layers deposited at 4000 and 8000 rpm a film thickness of ≈350 and 270 nm was obtained, respectively. Once the HPVK is properly deposited on the substrate PMMA is spin coated on the top the sample and post heated at 80 and 150 °C for 2 min each to develop sample B structure. The thickness of the polymer is controlled by the spin coating velocity or the concentration of polymer in the solvent (toluene).

Waveguide Characterization: Waveguides have been characterized at room temperature by end fire coupling the pump laser with the aid of a microscope objective. Excitation source consisted of a Nd:Yag laser (1 ns pulse, 20 KHz repetition rate) doubled at 533 nm with a nonlinear KTP crystal. Waveguided PL is collected at the output edge of the sample with another microscope objective and focused into a fiber optic connected to a HR4000 Ocean Optics spectrograph (estimated overall resolution better than 0.7 nm). Time resolved PL was carried out by focusing the PL into a Hamamatsu C5658-3769 avalanche photodetector connected to a BOXCARDPCS-150 electronics from Becker & Hickl GmbH.

Textural Characterization: SEM images of the substrate were carried out using a JSM-7000F JEOL 216 FEG-SEM system using secondary and retrodispersed electron beams.

Supporting Information

Supporting Information is available from the Wiley Online Library or from the author.

Acknowledgements

This work was supported by Generalitat Valenciana (Project No. ISIC/2012/008), the Universitat Jaume I (Project No. 12I361.01/1), Spanish MINECO (Projects Nos. MAT2013-47192-C3-1-R and TEC2014-53727-C2-1-R) and EU-NAVOLCHI (Project No. 288869). The authors would like to thank Prof. G. Lifante for his help in the implementation of the BPM algorithm.

Received: July 6, 2015
Revised: July 22, 2015
Published online:

[1] C. C. Stoumpos, C. D. Malliakas, M. G. Kanatzidis, *Inorg. Chem.* **2013**, *52*, 9019.

[2] a) M. Liu, M. B. Johnston, H. J. Snaith, *Nature* **2013**, *501*, 395; b) H.-S. Kim, C.-R. Lee, J.-H. Im, K.-B. Lee, T. Moehl, A. Marchioro, S.-J. Moon, R. Humphry-Baker, J.-H. Yum, J. E. Moser, M. Gratzel, N.-G. Park, *Sci. Rep.* **2012**, *2*, 591; c) A. Kojima, K. Teshima, Y. Shirai, T. Miyasaka, *J. Am. Chem. Soc.* **2009**, *131*, 6050; d) N. J. Jeon, J. H. Noh, Y. C. Kim, W. S. Yang, S. Ryu, S. I. Seok, *Nat. Mater.* **2014**, *13*, 897; e) A. Mei, X. Li, L. Liu, Z. Ku, T. Liu, Y. Rong, M. Xu, M. Hu, J. Chen, Y. Yang, M. Grätzel, H. Han, *Science* **2014**, *345*, 295; f) J.-H. Im, I.-H. Jang, N. Pellet, M. Grätzel, N.-G. Park, *Nat. Nanotechnol.* **2014**, *9*, 927; g) J. Burschka, N. Pellet,

S.-J. Moon, R. Humphry-Baker, P. Gao, M. K. Nazeeruddin, M. Gratzel, *Nature* **2013**, *499*, 316; h) H.-S. Kim, I. Mora-Sero, V. Gonzalez-Pedro, F. Fabregat-Santiago, E. J. Juarez-Perez, N.-G. Park, J. Bisquert, *Nat. Commun.* **2013**, *4*, 2242; i) J. T.-W. Wang, J. M. Ball, E. M. Barea, A. Abate, J. A. Alexander-Webber, J. Huang, M. Saliba, I. Mora-Sero, J. Bisquert, H. J. Snaith, R. J. Nicolas, *Nano Lett.* **2013**, *14*, 724.

[3] M. M. Lee, J. Teuscher, T. Miyasaka, T. N. Murakami, H. J. Snaith, *Science* **2012**, *338*, 643.

[4] M. A. Green, K. Emery, Y. Hishikawa, W. Warta, E. D. Dunlop, *Prog. Photovolt: Res. Appl.* **2015**, *23*, 1.

[5] L. Dou, Y. Yang, J. You, Z. Hong, W.-H. Chang, G. Li, *Nat. Commun.* **2014**, *5*, 5404.

[6] K. Chondroudis, D. B. Mitzi, *Chem. Mater.* **1999**, *11*, 3028.

[7] D. B. Mitzi, K. Chondroudis, C. R. Kagan, *IBM J. Res. Dev.* **2001**, *45*, 29.

[8] a) L. Gil-Escrig, G. Longo, A. Pertegas, C. Roldan-Carmona, A. Soriano, M. Sessolo, H. J. Bolink, *Chem. Commun.* **2015**, *51*, 569; b) Z.-K. Tan, R. S. Moghaddam, M. L. Lai, P. Docampo, R. Higler, F. Deschler, M. Price, A. Sadhanala, L. M. Pazos, D. Credgington, F. Hanusch, T. Bein, H. J. Snaith, R. H. Friend, *Nat. Nanotechnol.* **2014**, *9*, 687.

[9] Y.-H. Kim, H. Cho, J. H. Heo, T.-S. Kim, N. Myoung, C.-L. Lee, S. H. Im, T.-W. Lee, *Adv. Mater.* **2015**, *27*, 1248.

[10] E. R. Dohner, A. Jaffe, L. R. Bradshaw, H. I. Karunadasa, *J. Am. Chem. Soc.* **2014**, *136*, 13154.

[11] F. Deschler, M. Price, S. Pathak, L. Klintberg, D. D. Jarausch, R. Higler, S. Huettner, T. Leijtens, S. D. Stranks, H. J. Snaith, M. Atature, R. T. Phillips, R. H. Friend, *J. Phys. Chem. Lett.* **2014**, *5*, 1421.

[12] G. Xing, N. Mathews, S. S. Lim, N. Yantara, X. Liu, D. Sabba, M. Gratzel, S. Mhaisalkar, T. C. Sum, *Nat. Mater.* **2014**, *13*, 476.

[13] T. S. Kao, Y.-H. Chou, C.-H. Chou, F.-C. Chen, T.-C. Lu, *Appl. Phys. Lett.* **2014**, *105*, 231108.

[14] B. R. Sutherland, S. Hoogland, M. M. Adachi, C. T. O. Wong, E. H. Sargent, *ACS Nano* **2014**, *8*, 10947.

[15] a) J. Clark, G. Lanzani, *Nat. Photonics* **2010**, *4*, 438; b) Y. Koike, M. Asai, *NPG Asia Mater.* **2009**, *1*, 22.

[16] W.-J. Yin, T. Shi, Y. Yan, *Adv. Mater.* **2014**, *26*, 4653.

[17] A. Sadhanala, F. Deschler, T. H. Thomas, S. a. E. Dutton, K. C. Goedel, F. C. Hanusch, M. L. Lai, U. Steiner, T. Bein, P. Docampo, D. Cahen, R. H. Friend, *J. Phys. Chem. Lett.* **2014**, *5*, 2501.

[18] D. Amarasinghe, A. Ruseckas, G. A. Turnbull, I. D. W. Samuel, *Proc. IEEE* **2009**, *97*, 1637.

[19] C. Grivas, M. Pollnau, *Laser Photonics Rev.* **2012**, *6*, 419.

[20] C. Dang, J. Lee, C. Breen, J. S. Steckel, S. Coe-Sullivan, A. Nurmikko, *Nat. Nanotechnol.* **2012**, *7*, 335.

[21] a) V. I. Klimov, A. A. Mikhailovsky, S. Xu, A. Malko, J. A. Hollingsworth, a. C. A. Leatherdale, H. J. Eisler, M. G. Bawendi, *Science* **2000**, *290*, 314; b) F. Todescato, I. Fortunati, S. Gardin, E. Garbin, E. Collini, R. Bozio, J. J. Jasieniak, G. D. Giustina, G. Brusatin, S. Toffanin, R. Signorini, *Adv. Funct. Mater.* **2012**, *22*, 337.

[22] S. D. Stranks, S. M. Wood, K. Wojciechowski, F. Deschler, M. Saliba, H. Khandelwal, J. B. Patel, S. Elston, L. M. Herz, M. B. Johnston, A. P. H. J. Schenning, M. G. Debije, M. Riede, S. M. Morris, H. J. Snaith, *Nano Lett.* **2015**, DOI: 10.1021/acs.nanolett.5b00678.

[23] H. Zhu, Y. Fu, F. Meng, X. Wu, Z. Gong, Q. Ding, M. V. Gustafsson, M. T. Trinh, S. Jin, X. Y. Zhu, *Nat. Mater.* **2015**, *14*, 636.

[24] J. S. Manser, P. V. Kamat, *Nat. Photonics* **2014**, *8*, 737.

[25] E. Grilli, M. Guzzi, R. Zamboni, L. Pavesi, *Phys. Rev. B* **1992**, *45*, 1638.

[26] G. Lifante, *Integrated Photonics. Fundamentals*, John Wiley & Sons Ltd., Chichester, UK **2003**.

[27] H. Gordillo, I. Suárez, R. Abargues, P. Rodriguez-Canto, G. Almuneau, J. P. Martínez-Pastor, *J. Lightwave Technol.* **2013**, *31*, 2515.

[28] E. Rosencher, B. Vinter, *Optoelectronics*, Cambridge University Press, Cambridge, UK **2002**.

[29] G. Gordillo, I. Suárez, R. Abargues, P. J. Rodríguez-Cantó, J. P. Martínez-Pastor, *IEEE Photonics J.* **2013**, *5*, 220412.

Adv. Mater. **2015**,
DOI: 10.1002/adma.201503245